Percolation in suspensions of polydisperse hard rods: Quasi universality and finite-size effects

Hugues Meyer, Paul van der Schoot, and Tanja Schilling

Citation: The Journal of Chemical Physics **143**, 044901 (2015); doi: 10.1063/1.4926946
View online: http://dx.doi.org/10.1063/1.4926946
View Table of Contents: http://scitation.aip.org/content/aip/journal/jcp/143/4?ver=pdfcov
Published by the AIP Publishing

Percolation in suspensions of polydisperse hard rods: Quasi universality and finite-size effects

Hugues Meyer,[1] Paul van der Schoot,[2,3] and Tanja Schilling[1]
[1]*Research Unit for Physics and Materials Science, Université du Luxembourg, L-1511 Luxembourg, Luxembourg*
[2]*Department of Applied Physics, Eindhoven University of Technology, P.O. Box 513, 3500 MB Eindhoven, The Netherlands*
[3]*Institute for Theoretical Physics, Utrecht University, Leuvenlaan 4, 3584 CE Utrecht, The Netherlands*

(Received 1 June 2015; accepted 7 July 2015; published online 22 July 2015)

We present a study of connectivity percolation in suspensions of hard spherocylinders by means of Monte Carlo simulation and connectedness percolation theory. We focus attention on polydispersity in the length, the diameter, and the connectedness criterion, and we invoke bimodal, Gaussian, and Weibull distributions for these. The main finding from our simulations is that the percolation threshold shows quasi universal behaviour, i.e., to a good approximation, it depends only on certain cumulants of the full size and connectivity distribution. Our connectedness percolation theory hinges on a Lee-Parsons type of closure recently put forward that improves upon the often-used second virial approximation [T. Schilling, M. Miller, and P. van der Schoot, e-print arXiv:1505.07660 (2015)]. The theory predicts exact universality. Theory and simulation agree quantitatively for aspect ratios in excess of 20, if we include the connectivity range in our definition of the aspect ratio of the particles. We further discuss the mechanism of cluster growth that, remarkably, differs between systems that are polydisperse in length and in width, and exhibits non-universal aspects. © *2015 AIP Publishing LLC.* [http://dx.doi.org/10.1063/1.4926946]

I. INTRODUCTION

Composite nanomaterials have long attracted attention because of their potential application, for instance, in electronics, display technology, and photovoltaics.[2] Of particular interest in this context are their heat and charge transport properties.[3] Adding a sufficient amount of electrically conductive nanoparticles, such as carbon nanotubes or graphene, to an insulating polymer matrix produces a conductive composite the conductivity of which can be tuned by the choice of filler type, filler loading, and processing.[4] For many technological applications, the minimum filler loading required to reach a conductive state, the so-called percolation threshold, is desired to be as low as possible.[5] Rod-like particles are particularly suitable for this kind of application since they present very low percolation thresholds.[6] For the purpose of the rational design of such materials, it is crucial to be able to describe and predict the percolation threshold of assemblies of filler particles and understand the underlying mechanisms of the buildup of the system-spanning network required for effective conduction.

In experimental reality, the properties of the filler nanoparticles are not always well controlled.[7] Indeed, they are usually chemically and otherwise polydisperse, that is, consist of a mixture of particles of different dimensions and conductive properties. This complexity makes prediction of the percolation threshold and of the network structure very difficult, not least because of the huge parameter space. In this paper, we present a simulation and theoretical study of percolation in dispersions of polydisperse nanorods, specifically allowing for hard core interactions and targeting aspect ratios that are of an intermediate range, i.e., not in the scaling limit.[8–10]

Even though we find qualitative agreement with work on polydisperse ideal (penetrable) rods[10] and very long hard rods[8,9] (showing that the percolation threshold obeys laws that within a good approximation depend only on a few moments of the full distributions functions), quantitatively our results are very different. In fact, we find strong deviations in the dependence of the percolation threshold on the appropriate measures for the mean aspect ratio and connectivity of the particles. Finally, we find that the network connectivity properties are affected differently by variabilities in length, diameter, and connectivity criterion.

It is important to point out that the model systems that have been studied in the literature so far usually capture only one or a few aspects relevant to experimental reality. A very large focus is on the particle shape, attractive interactions, and aspect ratio.[11] While there is a huge body of the literature dealing with monodisperse systems, relatively little attention has been paid to polydisperse systems.[11–27] Recently, Chatterjee[28] and Otten and Van der Schoot[8,9] have developed theories of continuum percolation that take polydispersity into account and predict universal scaling laws for the percolation threshold. These predictions have only to a small extent been tested numerically.

In a recent simulation study, Nigro and co-workers confirm that for hard and penetrable rods that are polydisperse only in length, the percolation threshold depends only weakly on the exact shape of the length distribution.[10] A similar finding was obtained by Mutiso and collaborators for mutually penetrable length and width polydisperse rods.[29] They also find that finite-aspect-ratio corrections on the predictions of Otten and Van der Schoot are quite significant up to aspect ratios of about 100.[8,9]

Here, we go considerably beyond the scope of earlier work and report on simulation results for three different types of polydispersity that we investigate separately. The coupling between different kinds of polydispersity, predicted to be relevant for many experimental systems,[9] is postponed to future work. We show that the different kinds of polydispersity exhibit non-trivial universal behaviour. We invoke a treatment of connectedness percolation theory of hard rods recently put forward by us,[1] which is aimed at predicting finite-aspect-ratio corrections rather than obtaining them phenomenologically from simulations, as was done in Ref. 29.

The remainder of this paper is arranged as follows. We present in Section II the methods implemented in the Monte-Carlo simulations. Section III deals with the derivation of our version of connectivity percolation theory for polydisperse spherocylinders, including the Lee-Parsons approximation. Finally, we focus in Section IV on both numerical and theoretical results, first about the percolation thresholds and then about the cluster mechanisms. We end the paper with conclusions and a summary of the main findings in Section V.

II. SIMULATION METHODS

We consider hard spherocylinders consisting of cylinders of length L_i and diameter D_i, each capped by two hemispheres of the same diameter. See Fig. 1. The particles are not allowed to overlap but do not directly interact with each other when they are not in contact. The corresponding interaction potential is therefore either zero or infinite, making their resulting equilibrium properties temperature independent. We initialize a simulation box in which around 10 000 spherocylinders are perfectly aligned and regularly placed on square lattices spaced from each other along the rod direction. At each simulation step, the particles are then randomly rotated and translated. Equilibration is monitored by computing the nematic order parameter, which is expected to reach a constant value at the equilibrium (0 in the isotropic phase). Once the system is equilibrated, we generate ca. 5000 independent configurations of the system and average all quantities of interest over those configurations. In order to detect overlapping particles efficiently, the box is divided into a fine grid,[30] where the unit cell length is chosen equal to the greatest rod diameter in the system, so that the computational cost increases linearly with the number of particles. This method is very fast but rather expensive in terms of memory.

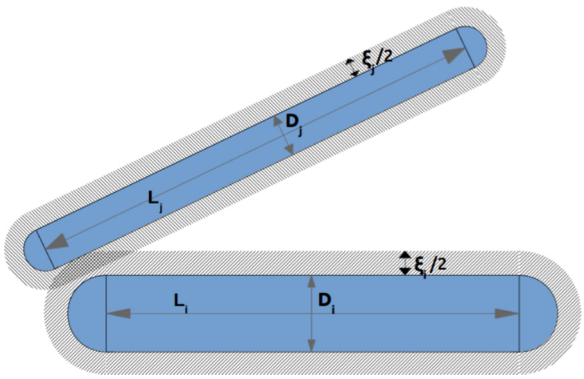

FIG. 1. Definition of the particle dimensions and connectivity range.

We take polydispersity into account by assigning to each rod a length and a diameter according to a probability density function $\mathcal{P}_L$ and $\mathcal{P}_D$. To generate a finite number of rods from a continuous distribution, we define an interval Δx where $x = L, D$ stands for length and width, and force the system to contain $N\mathcal{P}_x(x_0)\Delta x$ rods, whose dimension lies between x_0 and $x_0 + \Delta x$. This method turns out to give much more accurate results than simply drawing the rod dimensions directly from the distribution under study. In this work, the mean aspect ratio lies around $L/D = 15$ and the widest distributions we considered spread up to an aspect ratio of approximatively $L/D = 80$ for the very longest rods. In order to clearly distinguish between the effects of length and diameter polydispersity, we choose only uncorrelated distributions. As already advertised, this assumption does not necessarily apply to all experimental systems.

Connectedness percolation requires the definition of an inter-particle connectedness criterion. We define for each rod i a spherocylindrical shell of length L_i and diameter $D_i + \xi_i$ that contains the particle, where the connectivity parameter ξ_i obeys some distribution function $\mathcal{P}(\xi)$. Two particles are then connected if their surrounding shells overlap. Clusters are defined by contiguous pairwise connections. We define a configuration percolating if one of its clusters is connected to its image under periodic boundary conditions. To every configuration corresponds a percolation probability that is either 1 (it percolates) or 0 (it does not percolate), and averaging over many configurations, we compute a global continuous percolation probability for a particular system. A typical snapshot of such a sample and of its corresponding largest cluster is shown in Fig. 2.

In order to estimate the percolation threshold for a particular length, diameter, or connectivity distribution, we perform simulations using this distribution for a range of rod volume fractions. The volume fraction ϕ is defined with respect to the hard core volume of the particles and does not take into account the connectivity shell: $\phi = \frac{1}{a^3}\sum_{i=1}^{N} v_i$ where $v_i = \frac{\pi}{4}L_i D_i^2 + \frac{\pi}{6}D_i^3$ is the volume of the particle i, and a is the simulation box length. The percolation probability in a finite system is a sigmoidal function of the volume fraction running from 0 to 1. Its transition steepness increases with the box size and reaches a Heaviside step function in the limit of infinite box volume. The curves that correspond to different box volumes cross each other slightly below the concentration at which the probability reaches the value of 0.5. As we are interested in the scaling behaviour of the percolation threshold with the aspect ratio and cumulants of the size distribution of the particles, we do not need very accurate estimates. Hence, we ignore finite size effects and assume that the percolation threshold is the volume fraction corresponding to a percolation probability of 0.5. We verify that our box is sufficiently large to ensure that the percolation probability goes from 0.2 to 0.8 within a maximal volume fraction range $\Delta\phi_{max} = 0.005$. We assume this criterion to be restrictive enough for our results to achieve a satisfactory accuracy.

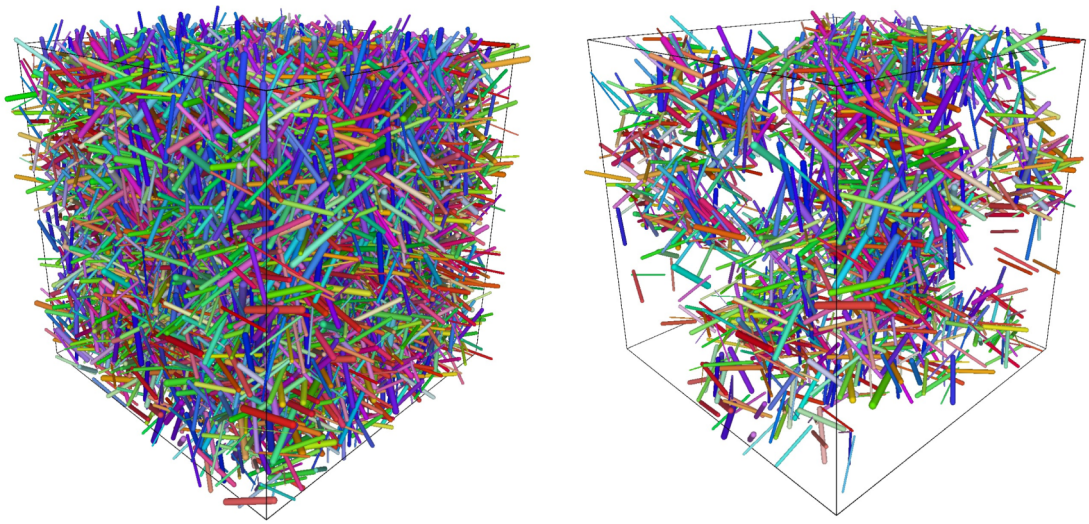

FIG. 2. Snapshot of an equilibrated configuration of diameter polydisperse spherocylinders at the critical volume fraction (left) and of the largest cluster within this particular configuration (right). Distribution is of the Weibull form $P(D) \propto \left(\frac{D}{\beta}\right)^{\alpha-1} e^{-(D/\beta)^{\alpha}}$ with $\alpha = 2.83$ and $\beta = 1.16$. Lengths and connectedness distances are all fixed to $L = 15$ and $\xi = 0.2$, respectively.

The effects of polydispersity on the percolation behaviour will also depend on the proximity of the system to phase transitions. On increasing concentration, spherocylindrical particles undergo a transition to the nematic phase, the orientational order of which influences the connectivity in the system. It is therefore a major concern to know if percolation is reached at a lower or higher density than the isotropic-nematic phase transition. This phenomenon has, for instance, been shown to be important in suspensions of percolating platelets.[31] However, ξ can be adjusted in order to lower or raise the percolation threshold, since it plays a role in the connectedness properties but not in the structure of the fluid. Our simulations were run with values of ξ that are in the order of the electron tunneling length in metallic fibres in composite materials. For these values, percolation always occurs in the isotropic phase.

III. THEORY

Percolation of clusters of nanoparticles in a fluid background medium can be investigated theoretically invoking what in essence is liquid state integral equation theory.[5] The theoretical framework is called connectedness percolation theory and it has been applied to hard and soft rod-like particles.[8,9,12] Here, we follow the same recipe, except that we will not rely on the second virial approximation that becomes exact in the limit of infinite aspect ratio. Instead, we opt for a closure that was recently shown to provide an accurate description of percolation of monodisperse, hard rods with an aspect ratio larger than roughly 10.[1]

Within the framework of connectedness percolation theory, the cluster size S can be expressed in terms of a function T, averaged over all of the attributes of orientation vector $\mathbf{u}$ and dimensions $\mathbf{x} \equiv (L, D, \xi)$ of the particles,[9]

$$S = \langle T(\mathbf{x}, \mathbf{u}) \rangle_{\mathbf{x},\mathbf{u}}. \tag{1}$$

The function T itself is a pair connectedness function averaged over its attributes and the solution of a generalised connectedness Ornstein-Zernike equation

$$T(\mathbf{x}, \mathbf{u}) - \rho \left\langle \hat{C}^{+}(0, \mathbf{x}, \mathbf{x}', \mathbf{u}') T(\mathbf{x}', \mathbf{u}') \right\rangle_{\mathbf{x}',\mathbf{u}'} = 1. \tag{2}$$

Here, ρ is the number density of particles and $\hat{C}^{+} = \hat{C}^{+}(\mathbf{q}, \mathbf{u}, \mathbf{u}')$, the spatial Fourier transform of the *connectedness* direct correlation function, that is, the direct correlation function for particles that are part of the same cluster, and $\mathbf{q}$ the wave vector. To average over the entire volume of the system, we have to take the zero wave vector limit, $\mathbf{q} \to 0$.

In the isotropic phase, the rods are randomly oriented, implying that $T(\mathbf{x}, \mathbf{u}) = T(\mathbf{x})$, which in turn allows us to redefine $\hat{C}^{+}$ as its average over the possible orientations, producing the simplified connectedness Ornstein-Zernike equation

$$T(\mathbf{x}) - \rho \left\langle \hat{C}^{+}(0, \mathbf{x}, \mathbf{x}') T(\mathbf{x}') \right\rangle_{\mathbf{x}'} = 1. \tag{3}$$

This equation needs to be closed and we follow Schilling *et al.*[1] by invoking the following ansatz: $\hat{C}^{+}(0, \mathbf{x}, \mathbf{x}') = \Gamma(\phi) \hat{f}^{+}(0, \mathbf{x}, \mathbf{x}')$.[1] Here, $f^{+} = e^{-\beta u^{+}}$ is the connectedness Mayer function and $\hat{f}^{+}$, its spatial Fourier transform,[9] with β the reciprocal thermal energy and u^{+} the so-called connectedness potential, and $\Gamma(\phi)$, a coefficient that depends on the volume fraction ϕ of the particles. For hard spheres, we write $C(r) = \Gamma(\phi) f(r)$ where the Mayer function $f(r)$ produces the second virial excess free energy if we choose as the reference state the zero density gas. $\Gamma(\phi)$ is chosen such that we reproduce the Carnahan-Starling equation of state. Therefore, the thermodynamics is at the level of Carnhan-Starling but the structure is that of a second virial fluid. Then, we make use of the identity $C = C^{+} + C^{*}$, with C^{+} the connectedness direct correlation function and C^{*} the blocking or disconnectedness direct correlation function. We furthermore have the identity $f = f^{+} + f^{*}$, which completes our derivation, giving $C^{+} = \Gamma(\phi) f^{+}$. The functional form of Γ is obtained from the Lee-Parsons expression for the excess free energy, interpolating between the Percus-Yevick equation of state for hard spheres and the Onsager equation of state for hard rods.[32–37] Similar closure relations have recently been developed by Chatterjee for disk

percolation.[38] Within this ansatz, we have

$$\Gamma(\phi) = \frac{1 - \frac{3}{4}\phi}{(1-\phi)^2}. \tag{4}$$

Notice that in the limit $\phi \to 0, \Gamma \to 1$ and we obtain the second virial theory that is valid in the Onsager limit of very slender rods. As we demonstrated recently,[1] corrections to the Onsager limit are significant for aspect ratios below a few hundreds.

For the case of hard rods, the connectedness Mayer function is 1 if the distance between two rods is between D and $\Delta \equiv D + \xi$ and 0 otherwise. The zero-wave vector Fourier transform of the connectedness Mayer function $\hat{f}^+(0, \mathbf{x}, \mathbf{x}')$ can be separated into contributions from interactions between the different portions of the spherocylindrical particles. We use Onsager's expression for the excluded volume of two hard spherocylinders to obtain[39]

$$\begin{aligned}\hat{f}^+(0,\mathbf{x},\mathbf{x}') = {} & LL'\frac{\Delta+\Delta'}{2}f_{11} + (L+L')\left(\frac{\Delta+\Delta'}{2}\right)^2 f_{10} \\ & + \left(\frac{\Delta+\Delta'}{2}\right)^3 f_{00} - LL'\frac{D+D'}{2}f_{11} \\ & - (L+L')\left(\frac{D+D'}{2}\right)^2 f_{10} - \left(\frac{D+D'}{2}\right)^3 f_{00}\end{aligned} \tag{5}$$

where $\Delta = D + \xi$ and the coefficients $f_{00} = 4\pi/3$, $f_{10} = \pi$, and $f_{11} = \pi/2$, respectively, indicate the cylinder-cylinder, cylinder-hemisphere and hemisphere-hemisphere contributions. Note that because u^+ is infinite for particles with overlapping hard cores and for those that are not connected, and zero for connected ones, $\hat{f}^+$ is essentially the difference between the excluded volume of two particles with hard-core radius Δ minus that of particles with hard-core radius D.

Let us first focus on length polydispersity alone, and set $D = D'$ and $\Delta = \Delta'$. In this particular case, Eq. (5) becomes

$$\hat{f}^+(L,L') = LL'\omega_1 f_{11} + (L+L')\omega_2 f_{10} + \omega_3 f_{00}, \tag{6}$$

where $\omega_n = \Delta^n - D^n$ are differences between powers of the interaction ranges Δ and D. Inserting this into Equation (3), we find

$$\begin{aligned}T(L) - \rho\Gamma(\phi)(L\omega_1 f_{11} + \omega_2 f_{10})\,\langle LT(L)\rangle_L \\ - \rho\Gamma(\phi)(L\omega_2 f_{10} + \omega_3 f_{00})\langle T(L)\rangle_L = 1.\end{aligned} \tag{7}$$

The two unknown coupled quantities are $\langle T(L)\rangle_L$ and $\langle LT(L)\rangle_L$; therefore, we need two independent equations relating them. The first one we obtain by averaging Equation (7), whereas the second we derive by first multiplying Equation (7) with L and averaging the resulting equation. As these relations are linear, we can summarize them by defining two vectors $\underline{X}$ and $\underline{Y}$ and a matrix $\underline{\underline{M}}$:

$$\begin{aligned}\underline{X} &= \begin{bmatrix}\langle T(L)\rangle \\ \langle LT(L)\rangle\end{bmatrix}, \quad \underline{Y} = \begin{bmatrix}1 \\ \langle L\rangle\end{bmatrix}, \\ \underline{\underline{M}} &= \begin{bmatrix}1-k\alpha_1 & -k\beta_1 \\ -k\alpha_2 & 1-k\beta_2\end{bmatrix}, \quad \underline{\underline{M}}\,\underline{X} = \underline{Y},\end{aligned} \tag{8}$$

where we use the notation $k \equiv \rho\Gamma(\phi)$, $\alpha_1 \equiv \langle L\rangle\omega_2 f_{10} + \omega_3 f_{00}$, $\alpha_2 \equiv \langle L^2\rangle\omega_2 f_{10} + \langle L\rangle\omega_3 f_{00}$, $\beta_1 \equiv \langle L\rangle\omega_1 f_{11} + \omega_2 f_{10}$, and $\beta_2 \equiv \langle L^2\rangle\omega_1 f_{11} + \langle L\rangle\omega_2 f_{10}$. The cluster size $S = \langle T(L)\rangle$ is the first element of $\underline{X} = \underline{\underline{M}}^{-1}\underline{Y}$. Each element of the matrix $\underline{\underline{M}}^{-1}$ is a fraction whose denominator is the determinant of $\underline{\underline{M}}$.

Therefore, S can be written as

$$S = \frac{\sum_{n,p,q} A_{npq}\langle L^n\rangle D^p \xi^q}{\det \underline{\underline{M}}}, \tag{9}$$

where A_{npq} are coefficients which involve the quantities k and f_{ij}. However, their exact expressions are not important for the remaining calculations, so we do not reproduce them here. The percolation threshold is the volume fraction ϕ_c for which S diverges, or, equivalently, that makes $\det \underline{\underline{M}} = 1 - k(\alpha_1 + \beta_2) + k^2(\alpha_1\beta_2 - \alpha_2\beta_1)$ vanish. Therefore, we determine ϕ_c by solving this simple second-order polynomial equation for k and by then relating k and ϕ, $\phi\Gamma(\phi) = k\langle v\rangle$, where $\langle v\rangle = \frac{\pi}{4}\left(\langle L\rangle D^2 + \frac{2}{3}D^3\right)$ is the average volume of a particle. The polynomial equation yields two solutions $k_\pm$. We define then $\gamma_\pm = k_\pm\langle v\rangle$.

The final equation that we have to solve is therefore

$$\left(\gamma_\pm + \frac{3}{4}\right)\phi_c^2 - (1 + 2\gamma_\pm)\phi_c + \gamma_\pm = 0, \tag{10}$$

which has two solutions for ϕ_c,

$$\phi_c = \frac{1 + 2\gamma_\pm \pm \sqrt{1+\gamma_\pm}}{2\gamma_\pm + \frac{3}{2}}. \tag{11}$$

We have four solutions for ϕ_c but we only keep the positive solution below unity for obvious physical reasons.

The analysis of the cases of diameter and connectedness polydispersity is completely analogous to that of length polydispersity, that is, the same method is applied starting from Eq. (5) setting $L = L'$ and $\xi = \xi'$, and $L = L'$ and $D = D'$, respectively. $\underline{\underline{M}}$ then turns into a 3×3 matrix for diameter polydispersity and a 4×4 one for connectedness polydispersity. This leads to third and fourth order polynomial equations that need to be solved. It is important to note that the percolation threshold will then explicitly depend on the higher order moments $\langle D^n\rangle$ with $n \le 4$ and $\langle \xi^m\rangle$ with $m \le 6$, respectively. To derive a theory for a system polydisperse in length, diameter, and connectedness simultaneously is possible, but it does not simplify Equation (5). Such calculations would therefore involve quantities of the form $\langle L^n D^p \xi^q\rangle$ and could handle correlated as well as uncorrelated distributions. However, for clarity of exposition, we decided to keep this for future work.

IV. RESULTS

A. Percolation thresholds

If we invoke the second-virial approximation and neglect the end-cylinder and end-end interactions, the percolation threshold, ϕ_c, becomes proportional to the reciprocal weight average length $\langle L\rangle_w^{-1} \equiv \langle L\rangle / \langle L^2\rangle$, the mean square width $\langle D^2\rangle$, and a measure for the mean reciprocal connectivity length $\left[\langle\xi\rangle + \sqrt{\langle\xi^2\rangle}\right]^{-1}$, depending on the type of polydispersity.[8–10] Although this approximation produces results that are not very accurate for aspect ratios that are not huge, it is useful to take it as a reference because it shows what cumulants of

the full distribution are expected to govern the percolation threshold. We note in this context that the nature of length and diameter polydispersity is fundamentally different from that of connectedness distance polydispersity. The first two relate to polydispersity in the particle dimensions and hence in the interactions between particles, whilst the third one is a polydispersity in the electrical connectivity length scale only, which does *not* affect the structure of the liquid but only the resulting cluster size distribution.

To separate these various effects, we define two new dimensionless quantities, being $\chi = \langle L\rangle_w/\sqrt{\langle D^2\rangle}$ and $\lambda = \left[\langle\xi\rangle + \sqrt{\langle\xi^2\rangle}\right]/2\sqrt{\langle D^2\rangle}$. The former, χ, becomes equal to either $\langle L\rangle_w/D$ or $L/\sqrt{\langle D^2\rangle}$ depending on the type of polydispersity and is analogous to the aspect ratio, as we cannot define a unique aspect ratio in polydisperse systems. The latter, λ, becomes $\left[\langle\xi\rangle + \sqrt{\langle\xi^2\rangle}\right]/2D$ for rods with a monodisperse diameter, and represents a characteristic connectedness shell thickness compared to the particle diameter. In addition, we derive an approximative expression of the percolation threshold as a function of both χ and λ,

$$\phi_c = \left[\frac{4}{3} + 2\lambda(\chi + 8)\right]^{-1}. \tag{12}$$

This expression is obtained within the context of length polydispersity, by first truncating the polynomial equation $\det \underline{\underline{M}} = 0$ at the first order in density in order to turn it into a trivial linear equation. This yields an approximative solution of the percolation threshold within the second virial approximation in which we only keep the leading order terms. Finally, we insert this expression into Equation (11) (in place of $\gamma_\pm$) in which we Taylor expand the square root up to the first order. Since we derived it from the context of length polydispersity, the final formula only contains $\langle L\rangle_w$, D, and ξ. However, we extrapolate it to diameter and connectedness polydispersity by replacing $\langle L\rangle_w/D$ by χ and ξ/D by λ, yielding Equation (12), which includes simultaneously the three types of polydispersity.

We compare the percolation threshold obtained from our simulations, predictions based on the theory presented in Sec. III and those from the second-virial theory for which $\Gamma = 1$, as a function of χ^{-1} for length and diameter polydispersity and as a function of λ^{-1} for connectedness polydispersity. For all three kinds of polydispersity, we tested bidisperse, Gaussian, and Weibull distributions. The first describes binary mixtures, the second seems relevant as Gaussian distributions are common in many fields of physics, and the third has been experimentally observed in polymer-fiber composites that are polydisperse in length.[40,41] The simulation data is listed in Tables I–III.

Fig. 3 shows the percolation threshold for the case of length polydispersity as a function of the inverse aspect ratio χ^{-1}. Both theory and simulations display a remarkable universal behaviour of the percolation threshold as a function of $\langle L\rangle_w$. The three different distributions that we tested are very different in shape, but we find that the percolation threshold is not sensitive to this if expressed in terms of the weight average length $\langle L\rangle_w$. This was also shown by Nigro *et al.*[10] for penetrable particles and in a more limited fashion for hard particles. We find that the Lee-Parsons theory and our simulation results

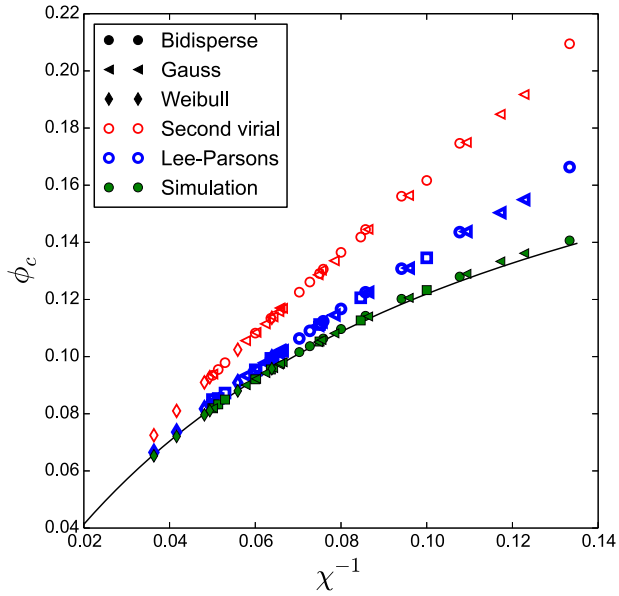

FIG. 3. Percolation threshold ϕ_c for length polydispersity as a function of the reciprocal aspect ratio $\chi^{-1} = D/\langle L\rangle_w$. Results are indicated from simulations (green full dots), Lee-Parsons theory (blue empty dots) as well as the second-virial approximation (red empty dots) for $\xi/D = 0.2$ and various distributions $\mathcal{P}(L)$ indicated by different symbols. A remarkable universal scaling with χ^{-1} is observed in the three cases. Simulation data are almost perfectly fit by Equation (12) (solid line). See also the main text.

quantitatively converge in the range $\chi > 20$ and are in qualitative agreement below that, whereas the theoretical prediction derived from the second virial approximation deviates notably even for relatively large aspect ratios. For monodisperse rods, the Lee-Parsons approach produces quantitative results already for $\chi > 10$.[1] Nevertheless, Equation (12) fits the simulation data surprisingly well, given the high level of approximation used to derive it. In polydisperse systems, the discrepancies between theory and simulations extend to larger average aspect ratios because of the shorter rods that are also present in the system. Note that the simulation results are always below the theoretical prediction. Hence, composite materials that contain fibres of short aspect ratio do not need as high filler loadings as theoretically expected in order to become conductive.

Also for diameter polydispersity, the second order cumulant is expected to be the most relevant one according to the second-virial theory, at least if we neglect end effects.[9] This is confirmed in Fig. 4 by both our simulation results and the more accurate predictions of Lee-Parsons theory albeit that we do not observe strictly universal behaviour. This suggests that higher order cumulants must be important too, at least for aspect ratios below 25. Remarkably, even the second-virial prediction yields results that are in almost quantitative agreement with the simulations for $\chi > 15$. The Lee-Parsons theory is in very good agreement with the simulation results even for relatively short particles. We note that this theory underestimates the percolation threshold for diameter polydisperse spherocylinders while it overestimates it for length polydisperse ones. Moreover, Equation (12) constitutes a very good estimation of the percolation threshold. However, we have to emphasize that this expression requires to be slightly rewritten in this particular case of diameter polydispersity, since λ is a

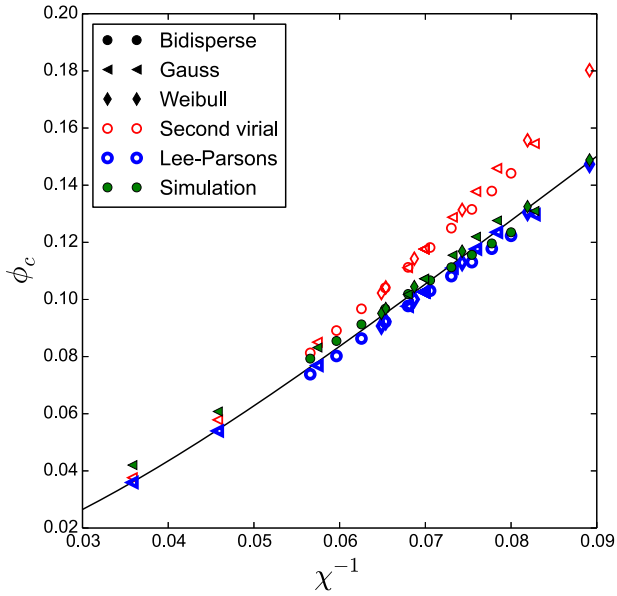

FIG. 4. Percolation threshold ϕ_c for diameter polydispersity as a function of $\chi^{-1} = \sqrt{\langle D^2 \rangle}/L$. Results are indicated from our simulations (green full dots), Lee-Parsons theory (blue empty dots) as well as the second-virial approximation (red empty dots) for $L/\xi = 75$ and various distributions $\mathcal{P}(D)$ indicated by different symbols. The scaling with χ^{-1} is not anymore universal, higher order cumulants matter. However, Equation (12) provides a very good approximation (solid line). See also the main text.

function of $\langle D^2 \rangle$ and therefore is not constant along the χ-axis. Indeed, one needs to replace λ by $\chi\xi/L$. Thus, the solid line corresponds to the function $\left[\frac{4}{3} + 2\frac{\xi}{L}\chi(\chi+8)\right]^{-1}$ where ξ and L are fixed.

Finally, we focus on connectedness distance polydispersity, illustrated in Fig. 5 for the case of an aspect ratio of

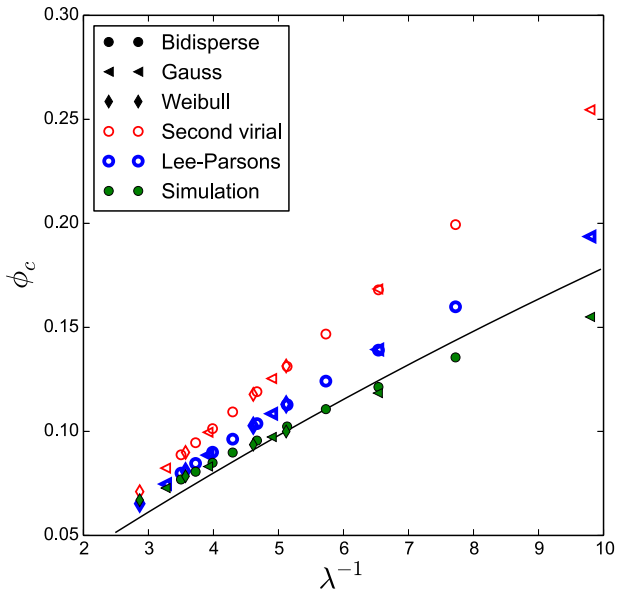

FIG. 5. Percolation threshold ϕ_c for polydispersity in the connectedness distance ξ, as a function of $\lambda^{-1} = 2D/\left[\langle\xi\rangle + \sqrt{\langle\xi^2\rangle}\right]$. Results from simulations (green full dots), Lee-Parsons theory (blue empty dots) as well as second-virial approximation (red empty dots) for $L/D = 15$ and various distributions $\mathcal{P}(\xi)$, indicated by different symbols. A universal scaling with λ^{-1} is also obtained. Additionally, Equation (12) gives a almost quantitative estimation of the percolation threshold (solid line). See also the main text.

15. As explained above, this does not lead to variability in the interactions between the particles, only in the definition of which particles are part of the same cluster. Nevertheless, it can be treated theoretically in the same way as the length and the diameter polydispersity due to the definition of the connectedness potential u^+. This explains why we find similar behaviour as for length and diameter polydispersity. Indeed, there is quasi-universal scaling with respect to λ, even though the aspect ratio is not all that large and one would expect higher order moments in the distribution of connectedness ranges to show up. Indeed, our calculations show contributions up to the sixth moment, $\langle\xi^6\rangle$, for the cluster size. Apparently, terms involving the first and second moments, $\langle\xi\rangle$ and $\langle\xi^2\rangle$, predominate the percolation threshold. Again, prediction from the second-virial approximation disagrees significantly with the simulations. The Lee-Parsons correction improves upon the quality of the prediction but still overestimates the threshold. Both theories improve for large values of λ, i.e., for globally thick connectedness shells for which the percolation threshold occurs at low volume fractions of particles. Our ansatz for the connectedness direct correlation function has by construction the spatial structure of a second virial theory, even though that our Lee-Parsons extension does have the thermodynamics that goes beyond it. Arguably, at higher densities, the actual structure of the direct correlation function starts to deviate from this. Note also that the Percus-Yevick prediction for the percolation threshold of monodisperse hard spheres is anyway in only qualitative agreement with simulations.[42] Nevertheless, Equation (12) provides again a satisfactory assessment of the percolation threshold in such kind of polydispersity. The quality of the fit is quite surprising since we derived it from equations of length polydispersity and extrapolated it to other type of polydispersities. In any event, it seems to be robust enough to be used for practical purposes.

B. Cluster formation mechanisms

As we have seen, the sensitivity of the percolation threshold to the higher order moments of the distribution function depends on the type of polydispersity: length, diameter, or connectedness range. It suggests that the mechanism by which the particles cluster differs between the different types of polydispersity. Indeed, hard particles of different size and/or shape have for entropic reasons a tendency to phase separate, and even if they do not actually phase separate this might give rise to fractionation of particles in the transient clusters that form in the mixtures.[43,44]

To investigate this, we compare in Fig. 6 the distribution of lengths and diameters within the largest cluster $\mathcal{P}_{\text{clus}}(x)$ with that in the entire system $\mathcal{P}(x)$ with $x = (L, D)$, for length and width polydisperse rods, respectively. In both cases, the larger particles are more abundant in the largest cluster than in the whole system, explaining why relatively small amounts of large particles have a large effect on the percolation threshold.[8] On the other hand, the effect weakens with increasing volume fraction of particles, at least for the length polydisperse ones. The proportion of short particles within large clusters is more and more important as packing fraction increases, making the gap between $\mathcal{P}_{\text{clus}}(x)$ and $\mathcal{P}(x)$ smaller.

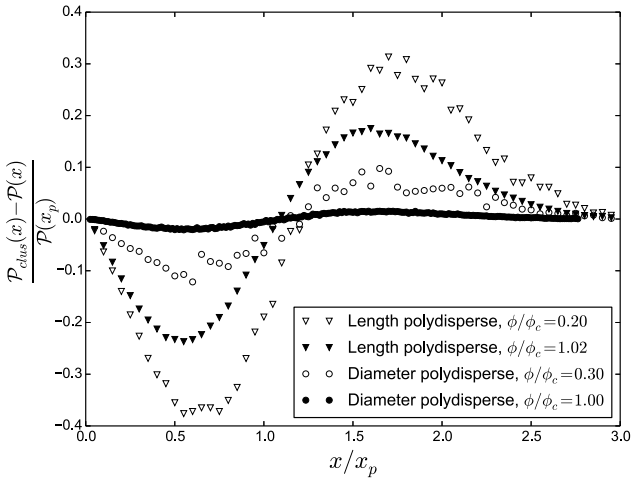

FIG. 6. Difference between the length and diameter distribution $P_{cluster}(x)$ of the largest cluster and the distribution $P(x)$ of the whole system, normalized by the value of the distribution at its peak, $P(x_p)$, as a function of the length $x = L$ or width $x = D$ scaled to the peak value, for two volume fractions in both cases. The length (triangles) and diameter (circles) distributions of the entire system are of the Weibull form $P(x) \propto \left(\frac{x}{\beta}\right)^{\alpha-1} e^{-(x/\beta)^{\alpha}}$ with $\alpha = 2.37$ and β being such that the distribution peaks lie at $L = 15$ and $D = 1$. Larger and thicker particles cluster more easily. The difference between the distributions within clusters and the global ones become smaller with increasing volume fraction. Notice that length polydispersity has a much stronger fractionation effect than diameter polydispersity.

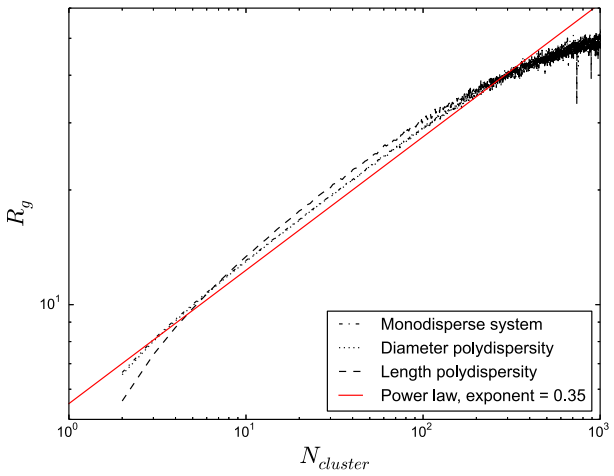

FIG. 7. Radius of gyration of clusters as a function of their size on a logarithmic scale for hard rods. Compared are results for monodisperse and for length and width polydisperse rods (see legend key). We set $D = 1$ and $L = 15$ in the monodisperse system. Length and width distributions are of the Weibull form $P(x) \propto \left(\frac{x}{\beta}\right)^{\alpha-1} e^{-(x/\beta)^{\alpha}}$ with $\alpha = 2$ and β chosen such that $\langle L \rangle_w = 15$ and $\langle D^2 \rangle = 1$ in both other systems. $\phi \simeq \phi_c$ and $\xi = 0.2$ in all three cases. Monodisperse systems as well as systems polydisperse in diameter superimpose and can be fitted by a power law exhibiting an exponent around 0.35 (deviations from this scaling for very large clusters are finite-size effects). This is not true for length polydispersity.

Another measure for the cluster structure is the fractal dimension d_f of the critical cluster. We obtain this by measuring the radius of gyration $R_f \sim N_{\text{cluster}}^{1/d_f}$ of the clusters as a function of the number of particles in it, N_{cluster}, see Fig. 7. This quantity is sensitive to length polydispersity and less to diameter polydispersity. The latter and that for monodisperse rods collapse exactly on the same curve that seems to exhibit a power law scaling and a fractal dimension of $d_f = 2.8$. Note that finite box-size effects cause deviations from pure power-law behaviour. For length polydisperse rods, we also do not find power law scaling but the trend seems to conform to the

TABLE I. Percolation thresholds computed from MC simulations for spherocylinders polydisperse in length, with $D = 1$ and $\xi = 0.2$.

Bidisperse distribution				Gaussian distribution			Weibull distribution		
L_1	L_2	p	ϕ_c	L_0	σ	ϕ_c	β	α	ϕ_c
10	20	0	0.082	8	1	0.136	23.50	1.80	0.065
10	20	0.1	0.083	8	2	0.133	21.39	1.98	0.072
10	20	0.2	0.085	8	3	0.129	19.37	2.27	0.080
10	20	0.5	0.092	10	2	0.121	19.14	2.55	0.081
10	20	0.6	0.095	10	4	0.114	17.52	2.82	0.088
10	20	0.8	0.105	10	6	0.106	16.06	4.10	0.096
10	20	0.9	0.113	10	8	0.097			
10	20	1.0	0.123	10	10	0.090			
5	15	0.2	0.102	12	3	0.108			
5	15	0.3	0.104	12	4	0.105			
5	15	0.4	0.106	15	1	0.098			
5	15	0.5	0.110	15	2	0.097			
5	15	0.6	0.114	15	3	0.096			
5	15	0.7	0.120	15	4	0.094			
5	15	0.8	0.128	15	5	0.092			
5	15	0.9	0.141						

TABLE II. Percolation thresholds computed from MC simulations for spherocylinders polydisperse in diameter, with $L = 15$ and $\xi = 0.2$.

Bidisperse distribution				Gaussian distribution			Weibull distribution		
D_1	D_2	p	ϕ_c	D_0	σ	ϕ_c	β	α	ϕ_c
0.8	1.2	0	0.123	0.4	0.32	0.042	1.01	11.703	0.095
0.8	1.2	0.1	0.120	0.6	0.32	0.060	1.04	5.53	0.097
0.8	1.2	0.2	0.116	0.8	0.32	0.083	1.09	3.65	0.104
0.8	1.2	0.3	0.111	1.0	0.32	0.107	1.17	2.82	0.117
0.8	1.2	0.4	0.107	1.2	0.32	0.130	1.26	2.37	0.132
0.8	1.2	0.5	0.1020	1.0	0.20	0.102	1.36	2.11	0.149
0.8	1.2	0.6	0.097	1.0	0.45	0.115			
0.8	1.2	0.7	0.091	1.0	0.52	0.122			
0.8	1.2	0.8	0.085	1.0	0.58	0.128			
0.8	1.2	0.9	0.079						

TABLE III. Percolation thresholds computed from MC simulations for spherocylinders polydisperse in connectedness range, with $L = 15$ and $D = 1$.

Bidisperse distribution				Gaussian distribution			Weibull distribution		
D_1	D_2	p	ϕ_c	ξ_0	σ	ϕ_c	β	α	ϕ_c
0.1	0.3	0.1	0.077	0.1	0.03	0.155	0.201	11.703	0.100
0.1	0.3	0.2	0.081	0.15	0.045	0.118	0.234	2.82	0.094
0.1	0.3	0.3	0.085	0.2	0.06	0.097	0.292	1.93	0.078
0.1	0.3	0.4	0.090	0.25	0.075	0.083	0.356	1.64	0.067
0.1	0.3	0.5	0.095	0.3	0.09	0.073			
0.1	0.3	0.6	0.102						
0.1	0.3	0.7	0.111						
0.1	0.3	0.8	0.121						
0.1	0.3	0.9	0.136						

same fractal dimension but with a larger prefactor. The fractal dimension of 2.8 is larger than the mean-field value of 2 we expect to hold for very long rods[45] and that we obtain from the second virial approximation, but close to the accepted value of 2.5 in three dimensions for standard percolation.[46] We expect that because in our simulations the aspect ratio of the particles is not very large that we find a deviation from the mean-field exponent.

We conclude that having varying lengths or diameters within a collection of hard rods does not fundamentally change the way percolation is reached. Still, the volume fraction at the percolation threshold is different from that for monodisperse rods, even if the average diameters (or lengths) are equal.

V. CONCLUSIONS

In summary, we have presented a theoretical and computer simulation study on the effects of polydispersity on the geometrical percolation in suspensions of hard spherocylinders. We compare results for bidisperse, Gaussian, and Weibull distributions and show that the percolation threshold is quite insensitive to the precise distribution. In the case of length and connectedness polydispersity, the thresholds superpose within numerical error when scaled with the appropriate second order cumulant of the size distribution. For diameter polydispersity, however, higher order moments seem to matter, as the superposition of the different distributions is not quite perfect. To analyse the simulation results, we also present a theoretical treatment of the problem within connectedness percolation theory that we find to quantitatively predict the percolation threshold for hard rods of aspect ratios above 20.

ACKNOWLEDGMENTS

This project was completed within the framework of the ARPE program of the École Normale Supérieure de Cachan, France. Data from computer simulations presented in this paper were carried out using the HPC facilities of University of Luxembourg.

APPENDIX: DEFINITION OF SIZE DISTRIBUTIONS

We report in Tables I–III the percolation thresholds computed from our simulations and plotted in this article. All values admit an error bar of $\Delta\phi = 0.002$. We recall the three distributions used (the gaussian is effectively a truncated gaussian distribution).

$$\begin{cases} \text{Bidisperse distribution} & \mathcal{P}(x) = p\delta(x - x_1) + (1-p)\delta(x - x_2) \\ \text{Gaussian distribution} & \mathcal{P}(x) = \dfrac{1}{\sigma\sqrt{\frac{\pi}{2}}\left(1 + \operatorname{erf}\left(\frac{x_0}{\sigma\sqrt{2}}\right)\right)} \exp\left(-\dfrac{(x-x_0)^2}{2\sigma^2}\right) \\ \text{Weibull distribution} & \mathcal{P}(x) = \dfrac{\alpha}{\beta}\left(\dfrac{x}{\beta}\right)^{\alpha-1} \exp\left(-\left(\dfrac{x}{\beta}\right)^{\alpha}\right) \end{cases}.$$

[1]T. Schilling, M. Miller, and P. van der Schoot, "Percolation in suspensions of hard nanoparticles: From spheres to needles," e-print arXiv:1505.07660 (2015).
[2]S. Park, M. Vosguerichian, and Z. Bao, "A review of fabrication and applications of carbon nanotube film-based flexible electronics," Nanoscale **5**(5), 1727–1752 (2013).
[3]B. Li and W. H. Zhong, "Review on polymer/graphite nanoplatelet nanocomposites," J. Mater. Sci. **46**(17), 5595–5614 (2011).
[4]M. Ghislandi, *Nano-Scaled Carbon Fillers and their Functional Polymer Composites* (Eindhoven University of Technology, Eindhoven, 2012).
[5]S. Torquato, *Random Heterogeneous Materials: Microstructure and Macroscopic Properties* (Springer, 2002), Vol. 16.
[6]C. Koning, M. C. Hermant, and N. Grossiord, *Polymer Carbon Nanotube Composites: The Polymer Latex Concept* (CRC Press, 2012).
[7]E. Tkalya, M. Ghislandi, R. H. J. Otten, M. Lotya, A. Alekseev, P. van der Schoot, J. Coleman, G. de With, and C. Koning, "Experimental and theoretical study of the influence of the state of dispersion of graphene on the percolation threshold of conductive graphene/polystyrene nanocomposites," ACS Appl. Mater. Interfaces **6**(17), 15113–15121 (2014).
[8]R. H. J. Otten and P. van der Schoot, "Continuum percolation of polydisperse nanofillers," Phys. Rev. Lett. **103**, 225704 (2009).
[9]R. H. J. Otten and P. van der Schoot, "Connectivity percolation of polydisperse anisotropic nanofillers," J. Chem. Phys. **134**(9), 094902 (2011).
[10]B. Nigro, C. Grimaldi, P. Ryser, A. P. Chatterjee, and P. van der Schoot, "Quasiuniversal connectedness percolation of polydisperse rod systems," Phys. Rev. Lett. **110**, 015701 (2013); e-print arXiv:1301.6006v1.
[11]T. Schilling, S. Jungblut, and M. A. Miller, "Networks of nanorods," in *Handbook of Nanophysics* (Taylor and Francis, 2009).
[12]A. V. Kyrylyuk and P. van der Schoot, "Continuum percolation of carbon nanotubes in polymeric and colloidal media," Proc. Natl. Acad. Sci. U. S. A. **105**(24), 8221–8226 (2008).
[13]Y. B. Yi and A. M. Sastry, "Analytical approximation of the percolation threshold for overlapping ellipsoids of revolution," Proc. R. Soc. London, Ser. A **460**(2048), 2353–2380 (2004).
[14]X. Wang and A. Chatterjee, "Connectedness percolation in athermal mixtures of flexible and rigid macromolecules: Analytic theory," J. Chem. Phys. **118**, 10787–10793 (2003).
[15]K. Leung and D. Chandler, "Theory of percolation in fluids of long molecules," J. Stat. Phys. **63**(5-6), 837–856 (1991).
[16]A. P. Chatterjee, "Continuum percolation in macromolecular fluids," J. Chem. Phys. **113**, 9310 (2000).
[17]S. H. Munson-McGee, "Estimation of the critical concentration in an anisotropic percolation network," Phys. Rev. B **43**, 3331–3336 (1991).
[18]A. Celzard, E. McRae, C. Deleuze, M. Dufort, G. Furdin, and J. F. Marêché, "Critical concentration in percolating systems containing a high-aspect-ratio filler," Phys. Rev. B **53**, 6209–6214 (1996).
[19]G. E. Pike and C. H. Seager, "Percolation and conductivity: A computer study. I," Phys. Rev. B **10**, 1421–1434 (1974).
[20]Z. Neda, R. Florian, and Y. Brechet, "Reconsideration of continuum percolation of isotropically oriented sticks in three dimensions," Phys. Rev. E **59**(3), 3717 (1999).

[21]M. Foygel, R. D. Morris, D. Anez, S. French, and V. L. Sobolev, "Theoretical and computational studies of carbon nanotube composites and suspensions: Electrical and thermal conductivity," Phys. Rev. B **71**, 104201 (2005).
[22]R. M. Mutiso and K. I. Winey, "Electrical percolation in quasi-two-dimensional metal nanowire networks for transparent conductors," Phys. Rev. E: Stat., Nonlinear, Soft Matter Phys. **88**(3), 032134 (2013).
[23]A. P. Chatterjee, "Geometric percolation in polydisperse systems of finite-diameter rods: Effects due to particle clustering and inter-particle correlations," J. Chem. Phys. **137**, 134903 (2012).
[24]L. Berhan and A. M. Sastry, "Modeling percolation in high-aspect-ratio fiber systems. I. Soft-core versus hard core models," Phys. Rev. E **75**(4), 041120 (2007).
[25]T. Schilling, S. Jungblut, and M. A. Miller, "Depletion-induced percolation in networks of nanorods," Phys. Rev. Lett. **98**(10), 108303 (2007).
[26]G. Ambrosetti, C. Grimaldi, I. Balberg, T. Maeder, A. Danani, and P. Ryser, "Solution of the tunneling-percolation problem in the nanocomposite regime," Phys. Rev. B **81**(15), 155434 (2010).
[27]B. Vigolo, C. Coulon, M. Maugey, C. Zakri, and P. Poulin, "An experimental approach to the percolation of sticky nanotubes," Science **309**, 920 (2005).
[28]A. P. Chatterjee, "Percolation thresholds for rod-like particles: Polydispersity effects," J. Phys.: Condens. Matter **20**(25), 255250 (2008).
[29]R. M. Mutiso, M. C. Sherrott, J. Li, and K. I. Winey, "Simulations and generalized model of the effect of filler size dispersity on electrical percolation in rod networks," Phys. Rev. B **86**(21), 214306 (2012).
[30]R. L. C. Vink and T. Schilling, "Interfacial tension of the isotropic–nematic interface in suspensions of soft spherocylinders," Phys. Rev. E **71**, 051716 (2005).
[31]M. Mathew, T. Schilling, and M. Oettel, "Connectivity percolation in suspensions of hard platelets," Phys. Rev. E **85**(6), 061407 (2012).
[32]J. D. Parsons, "Nematic ordering in a system of rods," Phys. Rev. A **19**(3), 1225–1230 (1979).
[33]S. D. Lee, "A numerical investigation of nematic ordering based on a simple hard rod model," J. Chem. Phys. **87**(8), 4972–4974 (1987).
[34]J. K. Percus and G. J. Yevick, "Analysis of classical statistical mechanics by means of collective coordinates," Phys. Rev. **110**(1), 1–13 (1958).
[35]E. Thiele, "Equation of state for hard spheres," J. Chem. Phys. **39**, 474–479 (1963).
[36]G. Cinacchi and F. Schmid, "Density functional for anisotropic fluids," J. Phys.: Condens. Matter **14**(46), 12223 (2002).
[37]M. Franco-Melgar, A. J. Haslam, and G. Jackson, "A generalisation of the onsager trial-function approach: Describing nematic liquid crystals with an algebraic equation of state," Mol. Phys. **106**(5), 649–678 (2008).
[38]A. P. Chatterjee, "Percolation thresholds for polydisperse circular disks: A lattice-based exploration," J. Chem. Phys. **141**(3), 034903 (2014).
[39]L. Onsager, "The effects of shape on the interaction of colloidal particles," Ann. N. Y. Acad. Sci. **51**(4), 627–659 (1949).
[40]S. Wang, Z. Liang, B. Wang, and C. Zhang, "Statistical characterization of single-wall carbon nanotube length distribution," Nanotechnology **17**(3), 634 (2006).
[41]P. J. Hine, H. R. Lusti, and A. A. Gusev, "Numerical simulation of the effects of volume fraction, aspect ratio and fibre length distribution on the elastic and thermoelastic properties of short fibre composites," Compos. Sci. Technol. **62**, 1445–1453 (2002).
[42]T. DeSimone, S. Demoulini, and R. M. Stratt, "A theory of percolation in liquids," J. Chem. Phys. **85**, 391 (1986).
[43]P. van der Schoot, "Structure factor of a semidilute solution of polydisperse rodlike macromolecules," Macromolecules **25**(11), 2923–2927 (1992).
[44]R. van Roij and B. Mulder, "Demixing versus ordering in hard-rod mixtures," Phys. Rev. E **54**(6), 6430 (1996).
[45]R. H. J. Otten and P. van der Schoot, "Connectedness percolation of elongated hard particles in an external field," Phys. Rev. Lett. **108**(8), 088301 (2012).
[46]D. Stauffer and A. Aharony, *Introduction to Percolation Theory* (CRC press, 1994).